Korean J. Chem. Eng., 35(7), 1441-1449 (2018)
DOI: 10.1007/s11814-017-0176-0

pISSN: 0256-1115
eISSN: 1975-7220

Purification of textile wastewater by using coated Sr/S/N doped TiO_2 nanolayers on glass orbs

Rozita Foulady Dehaghi*,†, Mohsen Behpour*, and Noshin Mir**

*Department of Analytical Chemistry, Faculty of Chemistry, University of Kashan, P. O. Box 87317-51167, Kashan, Iran
**Department of Chemistry, University of Zabol, P. O. Box 98615-538, Zabol, Islamic Republic of Iran
(*Received 3 May 2017 • accepted 24 June 2017*)

Abstract−Simultaneous doping of TiO_2 nanoparticles with three elements including Sr, S, and N is reported. The resulting material shows superior photocatalytic performance toward degradation of textile waste under visible and sunlight. The pure and doped TiO_2 nanolayers were prepared by sol-gel method and were fixed on a bed of glass orbs. The immobilized TiO_2 were characterized by a variety of techniques: X-ray diffraction (XRD), scanning electron microscopy (SEM), spectroscopy diffusion reflection (DRS), energy dispersive X-ray spectrometry (EDS) and elemental analysis (CHNS). The photocatalytic activity of the prepared fixed-bed materials toward degradation of the textile wastes was determined by using ultraviolet-visible spectroscopy (UV-Vis) and measurement of the chemical oxygen demand testing (COD). The best photocatalytic activity was observed with the use of Sr/S/N-TiO_2 nano-layers. Afterwards, the experimental conditions were optimized by tuning reaction parameters, including amount of doped metal ion on photocatalyst structure, sample solution pH and photoreactor output flow rate. The results confirmed that at natural pH 5.9 of sample solution, maximum decomposition of 91-99% of azo dyes was obtained in 8 h under visible irradiation. Finally, the experiments were repeated under 1.5 AM sunlight with high volume of reactants in order to confirm the cost-effectiveness of the designed photocatalyst.

Keywords: Sr/S/N-TiO_2, Photoreactor, Nanolayers, Textile Waste Photodegradation, Azo Dyes, Visible and Sunlight

INTRODUCTION

Among the most important sources of water pollution, industrial wastes are of great concern. Textile industry production of a wide range of polluting dye waste is considered one threatening polluting water industry [1,2]. Many studies have been done on purification methods of industrial wastewater containing hazardous substances such as azo dyes that are chemically stable and hardly biodegradable under aerobic conditions [3-5]. Wastewater treatment using advanced oxidation process is of the safest methods in this field [6,7]. This process is based on production of very active species such as hydroxyl radicals that leads to rapid and non-selective oxidation of whole range of organic pollutants [8,9]. After absorption of photons with proper energy, a photocatalyst is able to separate charges on its surface [10]. This phenomenon is based on electron excitation from the valence band to the conduction band of photocatalyst [11]. In this process, it is vital to prevent from recombination of produced electron-hole pairs in order to carry out reduction and oxidation processes using the produced hydroxyl radicals [12-15]. The use of photocatalytic processes in wastewater treatment operation has advantages such as complete mineralization, omitting waste disposal, low cost and ambient temperature and pressure conditions [16,17]. Titanium dioxide is one of the most promising photocatalysts because of its remarkable features such as non-toxicity, high stability, low cost and great efficiency in removing organic matters [18]. However, due to the wide band gap of TiO_2, its activation using visible or sun light needs a reform in its structure, because TiO_2 absorption takes place in the UV region. Since only 4% of sunlight contains ultraviolet light [20], many efforts have been devoted to narrowing TiO_2 band gap through metals or nonmetals doping [22]. For instance, N doping fulfills this aim through replacing its 2p orbitals with oxygen in the solid network [23].

Herein, we report triple doping of TiO_2 nanoparticles with metal and non-metal elements, Sr, S, and N. To our knowledge, there is not any previous report on simultaneous doping of these three elements. Co-doping Sr and Ag has been already reported and it has been shown that the recombination of photo-generated electrons and holes is effectively suppressed and the photocatalytic activity is increased by co-doping these elements [24]. Considering good performance of Sr as a dopant in TiO_2, its combination with two other important doping elements is investigated. In this work, first sol-gel method was used for synthesis of pure and doped titanium dioxide nanoparticles [25,26]. Second, the as-prepared nanoparticles were coated on glass orbs in order to achieve thin-film of photocatalysts since fixed bed photocatalysts do not require recovering and centrifuging after the process and therefore it is more appropriate for industrial use [27-29]. At the end, the photocatalytic activity of the prepared nano-layers was tested for degradation of azo dyes solution as a model of textile waste, under visible and sunlight in different conditions such as pH, various volumes of pollutants solution, difference output speed of photoreactor and optimum

†To whom correspondence should be addressed.
E-mail: r.foulady@gmail.com

amount of doped element.

MATERIALS AND METHODS

1. Materials and Reagents

Chemicals in this paper including tetrabutyl ortho titanate (Ti $(OC_4H_9)_4$ 98%), acetylacetone ($C_5H_8O_2$ 99%), hydrochloric acid (Hcl 37%), ethanol (C_2H_5OH 99%), Strontium Nitrate Hexahydrate ($Sr(NO_3)_2{\cdot}6H_2O$ 98%), thiourea (CH_4N_2S, as a source of nitrogen and sulfur) and other chemicals were analytical grade and purchased from Merck company (Germany) and used without any further purification. Deionized (DI) water that was prepared by an ultra-pure water system type smart-2-pure, TKA, Germany, was used throughout.

2. Synthesis and Immobilization of Pure and Doped TiO_2 Nanolayers on Glass Orbs

The preparation method of pure titanium dioxide sol is shown in Fig. 1. The doped TiO_2 nanoparticles were also prepared in the same way, except that 0.0153 g of strontium nitrate hexahydrate was dissolved in 2 ml of deionized water in step 3 and was added to the provided sol. Finally, for synthesis of Sr/N/S tri-doped TiO_2, in addition to adding certain amount of strontium nitrate hexahydrate according to previous method, after adjusting the pH of the solution, 0.25 g of thiuorea salt [30] was added to the sol solution and then put under final stirring.

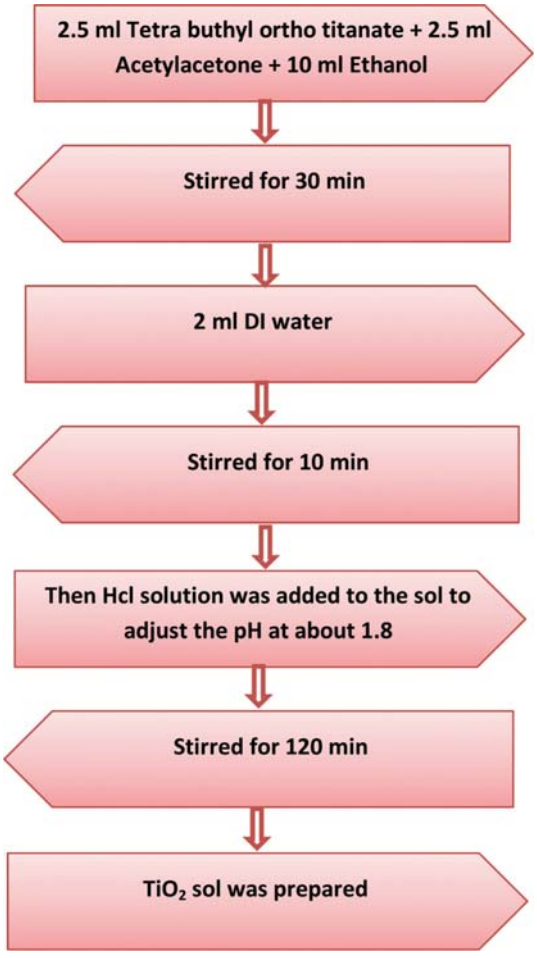

Fig. 1. Preparation of TiO_2 solution by sol-gel method.

After synthesis of the desired nanoparticles, immersion dip-coating method was used to produce a thin film of photocatalyst on the glass orbs surface (diameter 0.75 mm) as the photocatalyst substrate. For this purpose, the glass substrates were washed with a mixture of water and detergent and then were transferred in a solution of water and hydrochloric acid for 24 hours for cleaning. After preparation of the substrates, 13.8 g of glass orbs (the equivalent with three photoreactor tubes) were transferred into the sol solution and were out after 15 minutes and were dried with a hairdryer. This procedure was repeated two times, each time for 30 seconds, and finally the covered glass orbs were dried at 60 °C, for 4 h. Finally, the orbs were calcined at 500 °C, 1 hour. Eventually, the glass orbs were washed with distilled water to remove unattached burned materials from the surface and then were dried at 120 °C in electric oven for 1 h.

3. Photoreactor

In this study, the photocatalytic activity of pure TiO_2, Sr-TiO_2

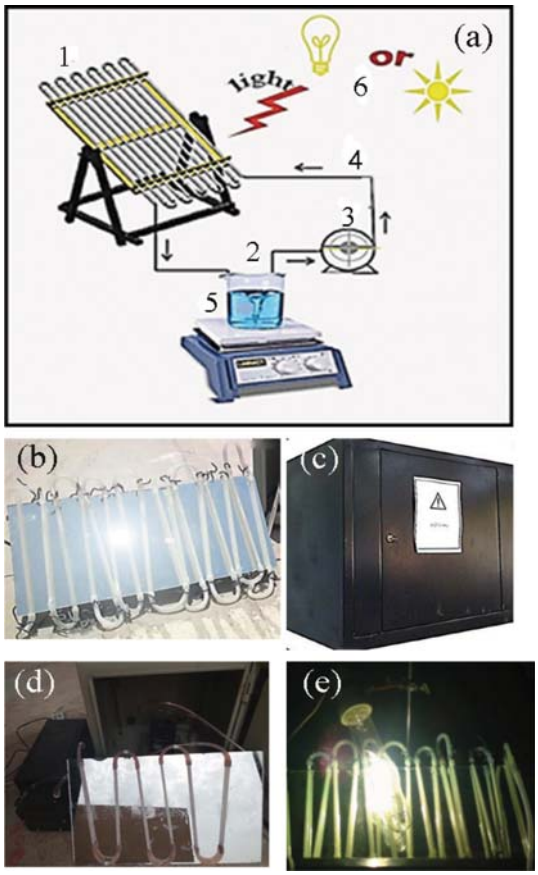

Fig. 2. (a) Schematic diagram of the experimental set, 1: photoreactor consisting of glass tubes assembled on a mirror, 2, 3, 4: dyes solution pumped to the photoreactor filled with deposited glass orbs, 5: dyes solution, 6: light sources. (b) photoreactor consisting of glass tubes assembled on a mirror, (c) the black box in which the experiment was done, (d) the ready set-up before experiment, (e) the running experiment inside the black box.

and Sr/S/N-TiO_2 nano-layers was investigated by continuous flow rate photoreactor in laboratory scale. This photoreactor consists of glass tubes (length 230 mm, internal diameter 7.50 mm), and is filled with the deposited glass orbs with photocatalytic substrates are placed in it. Each tube contains 4.60 g of deposited orbs. Then, all the tubes were connected in series, on the surface of a tilting mirror. An Osram lamp was used as a source of visible light. Peristaltic pumps (made in Iran), circulated the tested wastewater solution in the whole system, continuously. The entire system was placed inside a black box to avoid any external light in the system during the experiment. A schematic diagram of the set-up as well as the photos of reactor and experimental set-up in the black box are shown in Fig. 2.

4. Evaluation of Photocatalytic Activity

Photocatalytic efficiency of produced substrates was evaluated by examining the photodegradation of azo dye solution (as an example of textile waste), using photocatalytic system described in Section 2.2. For this purpose, a solution (25 mg/*l*) of a mixture of three azo dyes (Basic yellow 28, Basic red 46, Basic blue 41), was produced as a pollutant sample. The azo dye solution with a concentration of 25 ppm was used. Higher concentration of dye resulted in error in the absorption curve. The chemical structures of the azo dyes are shown in Scheme 1. The maximum absorption (λ_{max}) was at 453 nm, 538 nm and 606 nm for Basic yellow 28, Basic red 46 and Basic blue 28, respectively. Changes in the absorption of the sample solution during the photocatalytic process were evaluated using ultraviolet-visible spectroscopy (Lambda 2S, Perkin Elmer, Germany), at specified times (every 1 hour). Therefore, first, the maximum absorption of each dye was determined and changes in absorption after photocatalytic degradation were measured. Photocatalytic efficiency of azo dye solution was evaluated according to the following equation:

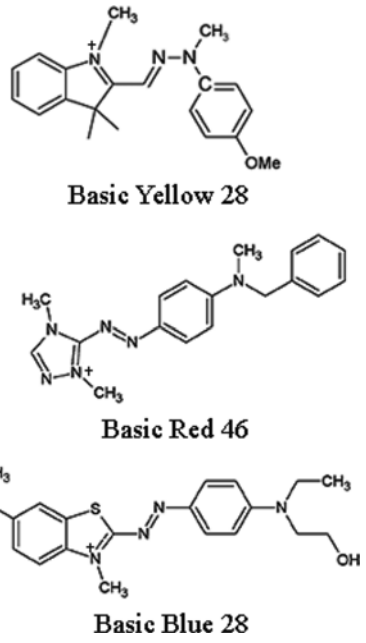

Scheme 1. Chemical structures of the azo dyes used in this work.

$$D\ (\%) = \frac{A_0 - A_t}{A_0}, \quad (1)$$

where D (%) is degradation percentage, A_0 is initial absorption of azo dyes solution and A_t is the absorption of sample solution at time t. The crystal size and crystalline form of the prepared thin films (in the powder form) were evaluated by a Philips X'pert Pro MPD model X-ray diffractometer using Cu Ka radiation as the X-ray source in the 2θ range of 10-80°. The average crystallite size of anatase phase was measured according to the Scherrer equation.

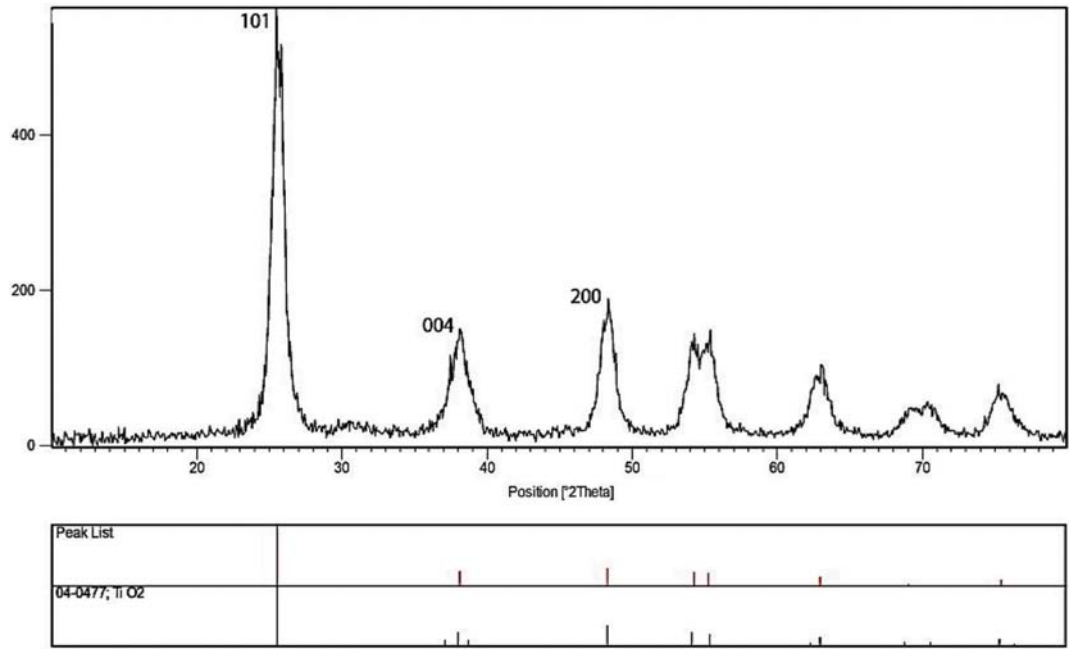

Fig. 3. XRD patterns of Sr/S/N-TiO_2 thin films.

The surface morphology of the TiO_2 films was observed using scanning electron microscopy (SEM) (Philips XL-30ESEM) equipped with energy dispersive X-ray. The amount of azo dye degradation was monitored using UV-Vis spectrophotometer (Perkin Elmer Lambda2S). Diffuse reflectance spectroscopy (DRS) (Shimadzu, model UV-3101) was used to investigate the energy gap changes. Also, in order to prove the presence of nitrogen and sulfur in the photocatalyst structure, elemental analysis (CHNS) (Elementar, Germany) was applied.

COD was determined via open reflux method according to (standard method for the examination of water and wastewater, section 5220-B). The quantity of oxidant consumed was expressed in terms of its oxygen equivalence. COD was measured using potassium dichromate solution (0.04 M) as an oxidant in strong acidic medium (sulfuric acid reagent) by reflux for 2 h. Then the remaining potassium dichromate was titrated with Ferroin indicator solution.

RESULTS AND DISCUSSION

1. X-ray Diffraction

The XRD patterns of Sr/S/N-TiO_2 (1% molar ratio of Sr/TiO_2 and 45% molar ratio of S-N/TiO_2) are shown in Fig. 3 in the 2θ range of 10-80°. Among the crystalline structure of titanium dioxide (anatase, rutile and Brookite), anatase shows the highest photocatalytic activity [31]. This is due to increase in trapping electron-holes on the surface of photocatalyst, and also it has a higher recovery potential for the production of electrons from inception to the end of the conduction band (anatase band gap is 0.1 eV more negative than rutile) [32-35]. As one can see, all the specified sharp peaks could be attributed to anatase TiO_2 according to the reported values (JCPDS: card No. 04-04770. The average particle size was calculated from the Scherrer equation on the anatase diffraction peaks:

$$D=K\lambda/\beta\cos\theta, \quad (2)$$

where D is the crystal size of the catalyst, λ is the X-ray wavelength, β the full width at half maximum (FWHM) of the diffraction peak (radian), K is equal to constant amount (0.89) and θ is the diffraction angle at the peak maximum. Average crystal sizes were calculated to be 17-18 nm, by using three peaks (101), (004) and (200) that were observed at 2θ of 25.46°, 38.01° and 48.02° for Sr/S/N-TiO_2 nanocrystalline powder.

2. Scanning Electron Microscopy

Fig. 4 shows the SEM images of Sr/S/N-TiO_2 thin films that were deposited on glass orbs. In Fig. 4(b) the film thickness is about 1.2 μm. Moreover, except for some parts of the film on which nanoparticles are slightly agglomerated, the film surface is uniform. The

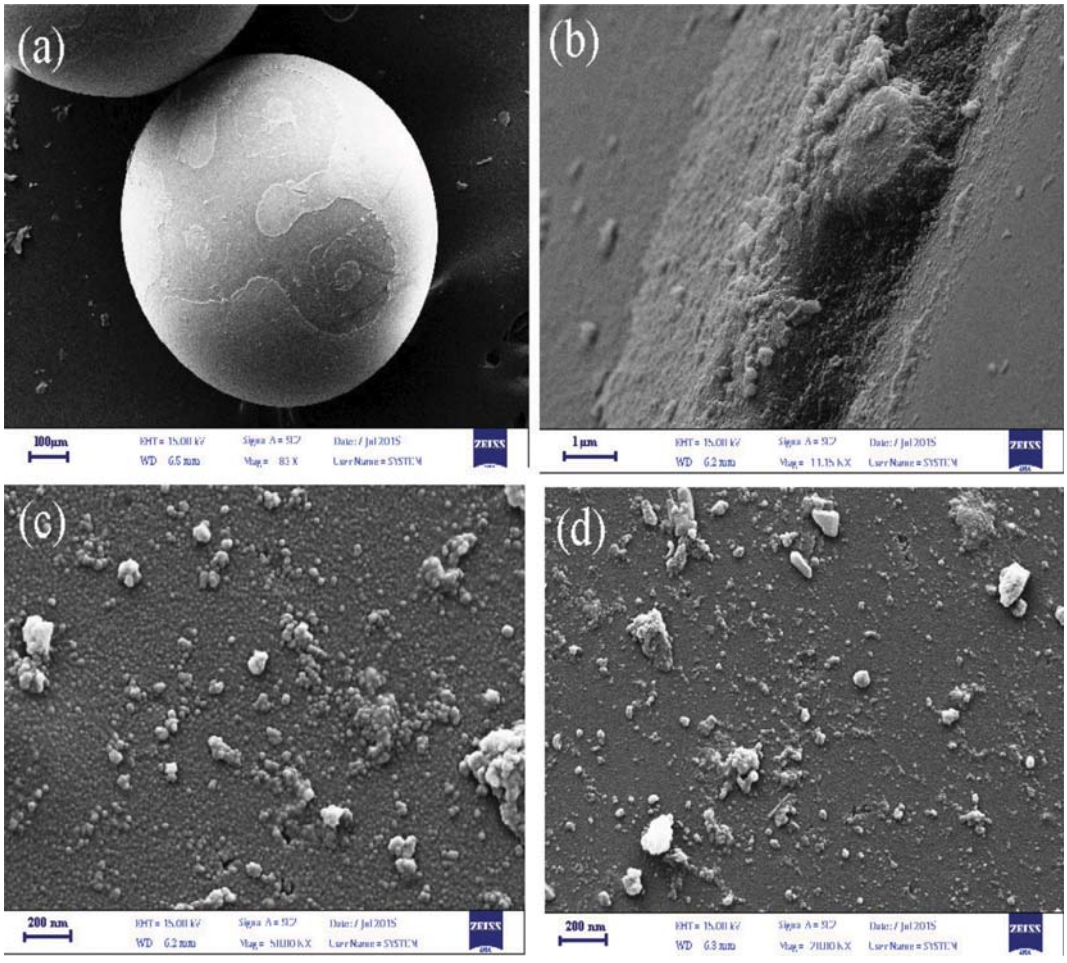

Fig. 4. SEM images of Sr/S/N-TiO_2 thin films deposited on glass balls in different scales: (a) 100 μm, (b) 1 μm, (c) 200 nm and (d) 200 nm.

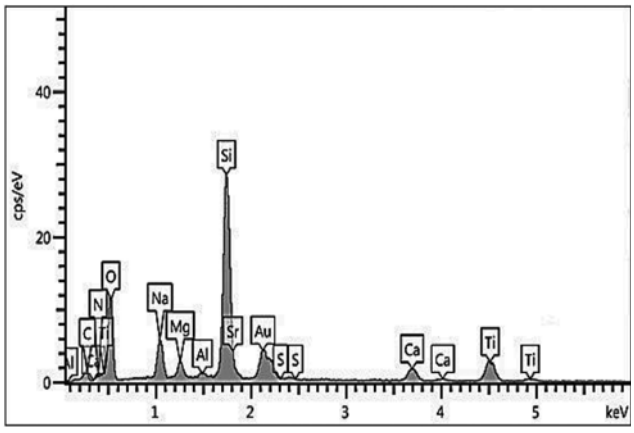

Fig. 5. EDS spectrum of Sr/S/N-TiO_2 thin film.

nanoparticles are spherical with the size of less than 50 nanometers.

3. Energy Dispersive Spectroscopy

EDS of Sr/S/N-TiO_2 is shown in Fig. 5. The presence of doping elements including strontium, sulfur, and nitrogen is confirmed by the corresponding peaks. Moreover, the peaks of Ti and O show the substrate composition. Other peaks related to Si, Na, Mg and C are because of the glass substrate and Au peak is related to the coated gold on the surface. Therefore, this result confirms the successful simultaneous doping of three metal and nonmetal elements in TiO_2 lattice.

4. Diffuse Reflectance Spectroscopy

To determine the energy gap of the prepared material, diffuse reflectance spectroscopy (DRS) was used. Electron transfer between the conduction band and valence band of anatase titanium dioxide is a kind of indirect transfer since its indirect band gap is smaller than its direct band gap and transition probability is according to

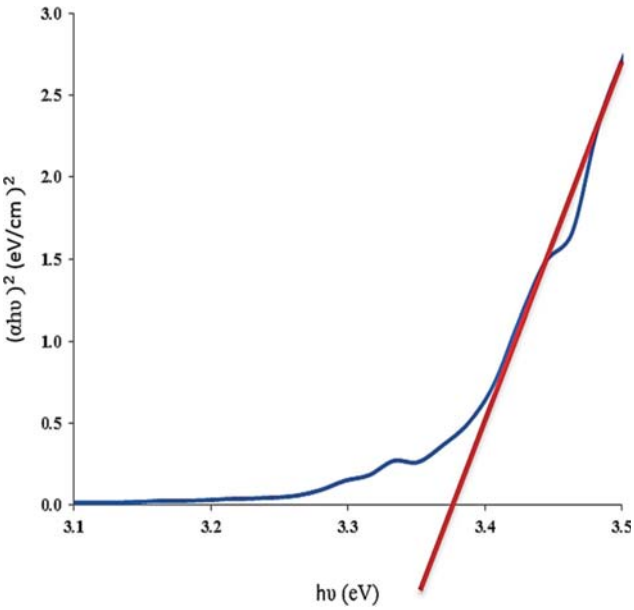

Fig. 6. DRS spectrum of Sr/S/N-TiO_2 thin film.

Table 1. CHNS analysis results

Wt% / Thin film	C%	H%	N%	S%
Sr/S/N-TiO_2	0.499	0.163	0.523	0.929

the following equation:

$$(\alpha h\upsilon)^2 = \alpha_0 (h\upsilon - E_g) \quad (3)$$

E_g represents the energy gap in this equation, hυ is amount of photon energy and α_0 is a constant. Gap energy also can be achieved by extrapolation of liner sector of graph to the photon energy. Fig. 6 shows the $(\alpha h\upsilon)^2$ terms of $h\upsilon$ graph of Sr/S/N-TiO_2 nanoparticles. The direct band gap energy of sample is about 3.93 eV. Given that the energy gap of titanium dioxide is 3.2 eV in bulk mode, can be acknowledged to reduce the particle size and conversion of bulk to the nanoscale.

5. CHNS Analysis

Using elemental analysis (CHNS), the presence and weight percentage of carbon, hydrogen, sulfur, and nitrogen were confirmed in doped TiO_2. The results are reported in Table 1. It can be observed that the amount of S and N was about 0.523 and 0.929% of the whole material.

6. Photocatalytic Activity of Photocatalyst under Visible Light

Photocatalytic activity of the all the prepared photocatalysts (pure TiO_2, and Sr/S/N-TiO_2) was evaluated by decomposition of azo dyes (25 mg/L, pH 5.9) aqueous solution under visible and sun light irradiation. A mixture of the three azo dyes was used as a model compound since they are the main components of the wastewater in the intinction processes [74-76]. Since the maximum absorption of these dyes is located in the visible region, their degradation can be easily monitored by UV-vis spectroscopy. The

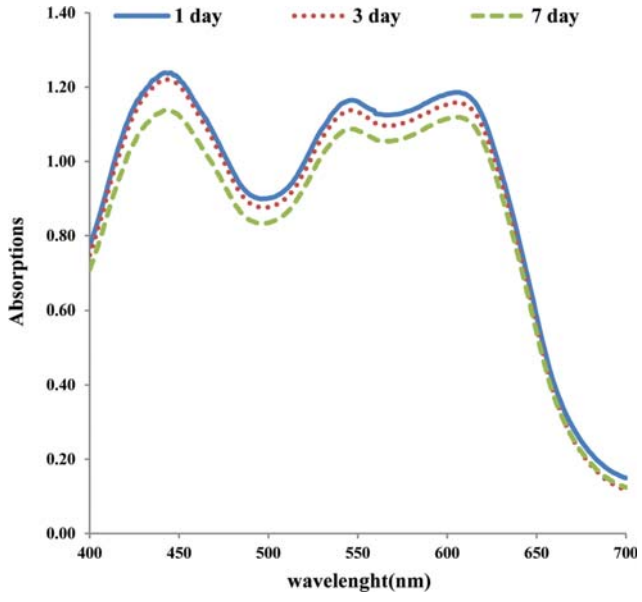

Fig. 7. Photodegradation of azo dyes solution in absence of photocatalyst and only by visible light irradiation (initial volume: 150 ml, pH: 5.9).

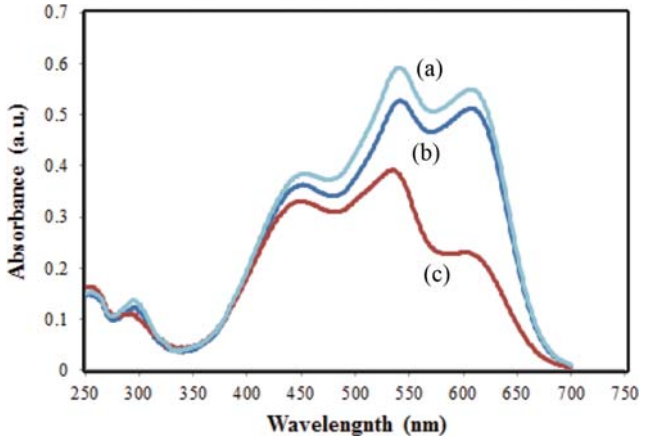

Fig. 8. Photodegradation of azo dyes solution (a) initial dye solution before experiment, (b) in presence of photocatalyst in dark, (c) in presence of photocatalyst under visible light irradiation (initial volume: 150 ml, pH: 5.9, time: 1 h).

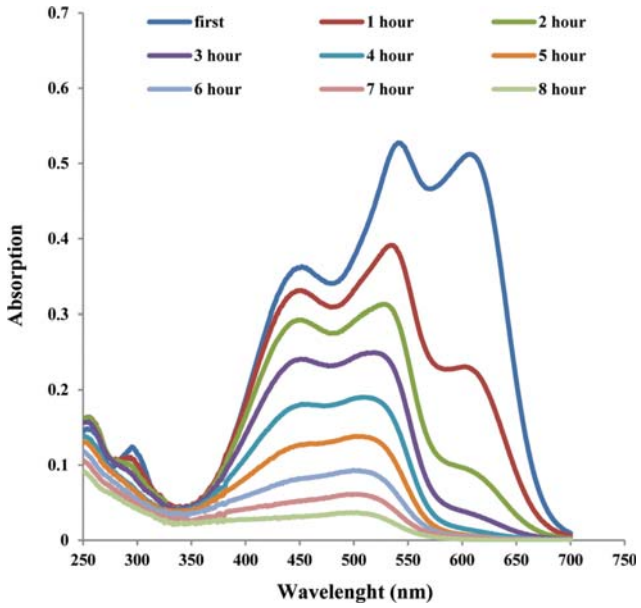

Fig. 9. Absorbance spectra of azo dyes solution as a function of time in the presence of Sr/S/N-TiO_2 thin films (initial volume: 150 ml, flow rate; 32 ml/min, pH: 5.9 static phase amount: 170.48 cm^2/g).

degradation process of azo dyes includes several steps in which the produced OH free radicals attack the azo structure and break -N=N- bond down. Consequently, azo dye molecules decompose and form smaller molecules, which finally, these molecules are oxidized to nontoxic CO_2 and H_2O [77]. Here, first, dyes were exposed to visible light for seven days without using photocatalyst and after seven days, no significant change was observed in the spectrum (Fig. 7). As a result, it can be acknowledged that the destruction of azo dyes in the absence of photocatalysis and just by visible light irradiation is not possible.

To differentiate dye adsorption and dye degradation properties of the introduced photocatalyst, two different experiments were devised. In the first one, dye solution was passed through photocatalyst without any illumination for one hour. In the second one, the same experiment was performed under visible illumination. Fig. 8 shows the obtained absorption spectrum after each experiment. Fig. 8(a), 8(b), and 8(c) show the absorption spectra of initial dyes solution, the solution after passing through the photocatalyst in dark, and the solution after passing through the photocatalyst under illumination, respectively. Since the first experiment was under dark condition, the observed decrease in the absorption spectrum could be mainly attributed to dye adsorption on the surface of the photocatalyst. In the second experiment, degradation under visible light is the main reason for decreasing dye concentration. Photodegradation mechanism of adsorbed dyes on the surface of photocatalysts can be explained this way:

$$TiO_2+h\upsilon\,(UV)\rightarrow TiO_2\,(e_{CB-}+h_{VB+}) \quad (4)$$

$$TiO_2\,(h_{VB+})+H_2O\rightarrow TiO_2+H^++OH^{\bullet} \quad (5)$$

$$TiO_2\,(h_{VB+})+OH^-\rightarrow TiO_2+OH^{\bullet} \quad (6)$$

$$TiO_2\,(e_{CB-})+O_2\rightarrow TiO_2+O_2^{-\bullet} \quad (7)$$

$$O_2^{-\bullet}+H^+\rightarrow HO_2^{\bullet} \quad (8)$$

$$Dye+OH^{\bullet}\rightarrow \text{degradation products} \quad (9)$$

$$Dye+h_{VB+}\rightarrow \text{oxidation products} \quad (10)$$

$$Dye+e_{CB-}\rightarrow \text{reduction products} \quad (11)$$

where, $h\upsilon$ is the necessary photon energy to excite the semiconductor electron from the valence band (VB) to conduction band (CB) [19]. Also, a similar test was performed in presence of pure titanium dioxide nanolayers; however, due to restrictions of TiO_2 in visible region, only 20-60 percentage of the sample was degraded after eight hours of irradiation. On the other hand, Sr-TiO_2 and Sr/S/N-TiO_2 resulted in degradation of 70-100 and 91-100%, respectively. This is due to the orbitals combination of doped elements, with the orbitals of titanium dioxide components, which led to the creation of new energy levels in the band gap of TiO_2 [36,37]. Also, it has been proven that doping TiO_2 with strontium ions causes inhibition of recombination of photogenerated charge carriers, leading to high quantum efficiency [38]. Changes in absorption spectra of azo dyes solution by using Sr/S/N-TiO_2 photocatalyst are shown in Fig. 9 as the best photocatalyst in visible region. Therefore, in this study, Sr/S/N-TiO_2 nanolayers were selected as the best photocatalysts with the highest activity and other reaction parameters were tuned to improve the performance of this catalyst.

7. The Effect of Sr Concentration on Photocatalytic Activity of Photocatalyst

To evaluate the effect of the concentration of doped-strontium in titanium dioxide structure on its photocatalytic response rate, TiO_2 nanolayers containing 0.5, 1.0 and 2.0 molar percent of Sr (in the presence of a constant amount of thiourea as a source of nitrogen and sulfur) were prepared and the photocatalytic activities were evaluated under visible light. The results shown in Table 2 demonstrate the prior performance of the sample containing 1.0% of Sr with over 90% degradation efficiency towards the azo dyes;

Table 2. Results of photodegradation percentage of sample solution on various amounts of Sr/TiO_2 molar ratio

Degradation of dyes \ Sr/TiO_2 molar ratio	0.5	1.0	2.0
Basic yellow 28	59.0%	91.0%	73.0%
Basic red 46	81.0%	96.0%	85.0%
Basic blue 41	92.0%	99.0%	95.0%

lower amount of doped Sr. Therefore, this concentration was chosen for other experiments in this work.

8. Optimization of Dye Solution pH

As an important and critical parameter in photocatalytic reactions, pH of the solution was selected for investigation. Therefore, degradation of the azo dye solution under UV-vis light in presence of Sr/S/N-TiO_2 was studied in different pH (2.0, 4.1, 5.9, 7.0, 8.0, 9.5). pH has a significant effect on the adsorption process because it determines the surface zeta potential of the material [39, 40]. Sodium hydroxide and hydrochloric acid were used to adjust the pH to alkaline and acidic pH values, respectively. The presented results in Fig. 10 show that the photodegradation percentage is higher in alkaline environment. This can be attributed to the structure of cationic dyes. The employed azo dyes in this study have surfaces with positive charge and also anatase TiO_2 has a positive zeta potential at pH ranges lower than 6 [41]. Therefore, there is an electric repulsion force between TiO_2 surface and azo dyes at acidic pH. On the other hand, at pH higher than 6, TiO_2 zeta potential is shifted to negative values, and thus an electric attraction force is created for positive dye adsorption on TiO_2 surface.

Moreover, it can be observed that Basic yellow 28 was less degraded at acidic pH=2 than two other dyes. This difference could

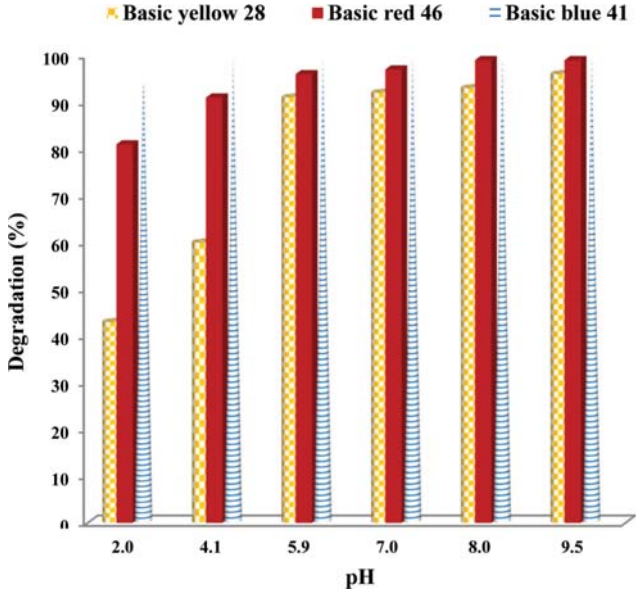

Fig. 10. Photodegradation efficiency of azo dyes solution with Sr/S/N-TiO_2 thin films in difference pH of sample solution (initial volume: 150 ml, flow rate; 32 ml/min, static phase amount: 170.48 cm^2/g).

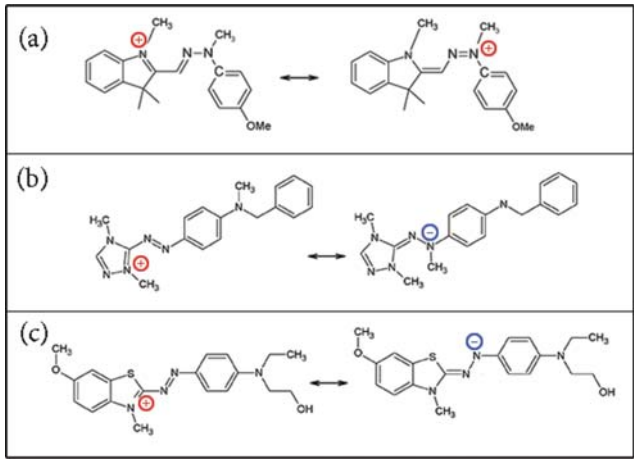

Scheme 2. Resonance forms of (a) basic yellow 28, (b) basic red 46, and (c) Basic blue 28.

be attributed to the possible resonance forms of three different dyes (Scheme 2). By drawing two different resonance forms of the dyes, it is observed that Basic yellow 28 has two different resonance form, which both of them are cationic. However, Basic red 46 and Basic blue 28 have two resonance forms, which one is anionic and the other one is cationic. Therefore, it is more likely that in acidic pH, the instantly formed anionic structures of two later dyes are absorbed on TiO_2 surface with positive potential zeta due to electrostatic forces and be degraded. Thus, in acidic pH, Basic red 46 and Basic blue 28 dyes are more degraded than Basic yellow 28 dye.

9. Effect of Flow Rate

Azo dye solution flow rate over the photocatalytic substrate was tuned to see the effect of contact time between dye and photocatalyst. For this purpose, three similar photoreactor tubes containing Zn/Tu-TiO_2 nanolayers coated on glass balls (150 ml of contamination sample) were exposed to three different flow rates of same dye solutions (20, 32 and 42 mL/min), and the experiment was performed under visible light irradiation. The absorption spectrum was recorded every hour. The results in Table 3 show that the highest degradation efficiency was obtained at 32 ml/min flow rate. It shows that at the flow rate of 20 mL/min, although the contact time is sufficiently high, due to low number of molecules passing over the photocatalyst the efficiency is not convincing. On the other hand, at the flow rate of 40 mL/min, it seems that the flow rate is so high that it does not provide enough contact time for complete degradation reaction. Therefore, 32 mL/min is the best flow rate which results in the best degradation efficiency.

Table 3. Results of photodegradation percentage of sample solution on difference output flow rate (ml/min)

Degradation of dyes \ Deby (ml/min)	20.0	32.0	42.0
Basic yellow 28	55.0%	91.0%	66.0%
Basic red 46	81.0%	96.0%	93.0%
Basic blue 41	95.0%	99.0%	99.0%

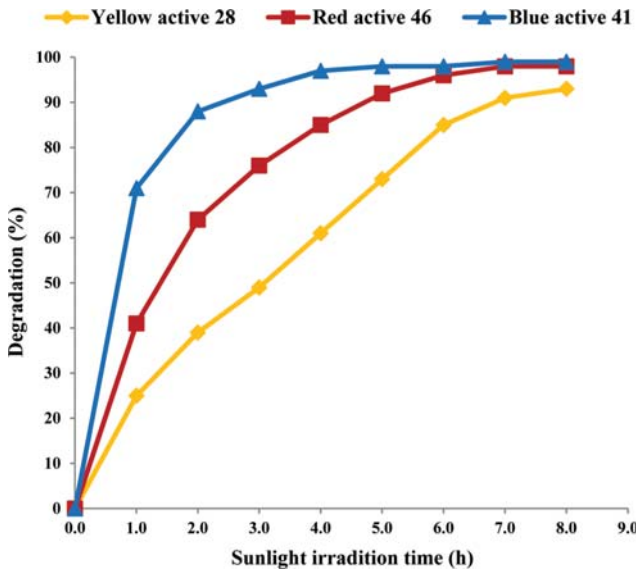

Fig. 11. Photodegradation effectiveness of azo dyes in the presence of Sr/S/N-TiO_2 thin films under Sunlight irradiation (initial volume: 150 ml, flow rate; 32 ml/min, pH: 5.9 static phase amount: 170.48 cm^2/g).

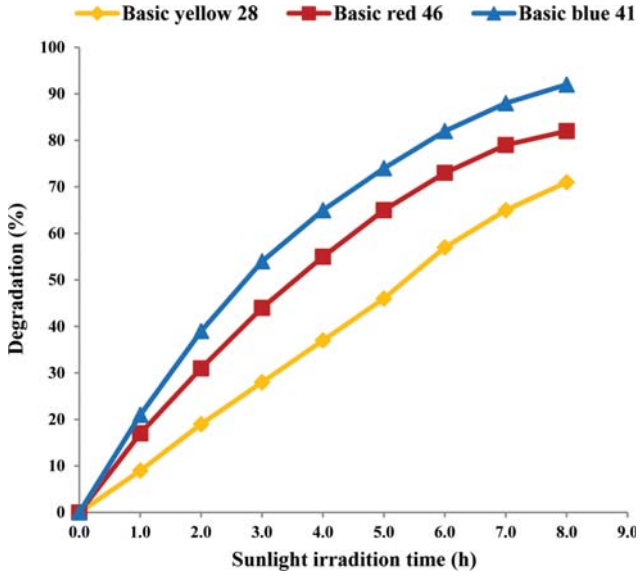

Fig. 12. Photodegradation effectiveness of azo dyes in the presence of Sr/S/N-TiO_2 thin films under Sunlight irradiation (initial volume: 600 ml, flow rate; 32 ml/min, pH: 5.9 static phase amount: 340.92 cm^2/g).

10. Stability and Repeatability of Photocatalytic Substrate

Stability after certain reaction cycles is a vital factor for selecting a photocatalyst especially for industrial application. Herein, the stability of the photocatalyst was tested for ten eight hour cycles. The obtained result shows that the efficiency of the photocatalyst is almost the same after ten cycles and photodegradation efficiency of 90-100% for each dye was achieved. The advantage of the prepared fix-bed photocatalyst is that it does not require any filtration or centrifugation after each cycle.

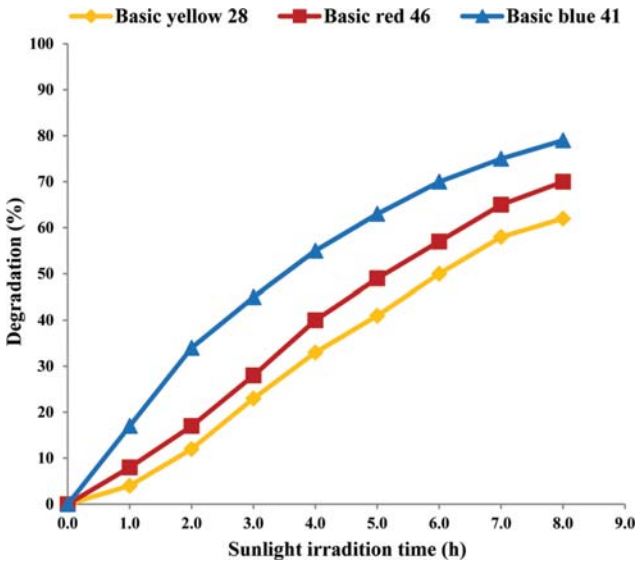

Fig. 13. Photodegradation effectiveness of azo dyes in the presence of Sr/S/N-TiO_2 thin films under Sunlight irradiation (initial volume: 1,100 ml, flow rate; 32 ml/min, pH: 5.9 static phase amount: 340.92 cm^2/g).

11. Photocatalytic Activity under Sunlight Irradiation

Finally, sunlight simulation as a natural and biocompatible source was used for photodegradation of azo dyes in presence of Sr/Tu-TiO_2 photocatalyst. For industrial purposes, a higher volume of the dye solution was prepared for the test. To perform this test, 150 ml of pollutants solution was passed through three similar test tubes containing the photocatalyst balls. Higher volumes of the pollutant solutions (600 and 1,100 ml) were tested in the fixed amount of photocatalysts (340.92 cm^2/g) for 8 hours. The results are shown in Fig. 11, Fig. 12 and Fig. 13, for 150, 600, and 1,100 mL of the solutions, respectively. The results show that replacing visible light with sunlight irradiation results in a slight increase in the degradation efficiency, which can be attributed to the higher intensity of visible light in sunlight (93-99% for 150 mL). However, as could be predicted, increasing the solution volume has an adverse effect on degradation percentage of dyes (71-92% for volumes of 600 ml and 62-79% for volumes of 1,100 ml). Some strategic modification such as increasing photocatalyst amount or employing bigger substrate could be useful for efficient degradation of high volumes

12. COD Investigation

COD is the standard method for measuring the amount of organic matter in wastewater. The purpose of this test is to ensure the complete degradation of pollutants. After irradiating with visible and sunlight for eight hours, COD value decreased from 190 to 55 and 51 mg/*l*, respectively, which shows excellent possibility of utilizing photocatalyst system in water decontamination.

CONCLUSION

Sr-TiO_2 and Sr/N/S-TiO_2 thin films were used to effectively degrade azo dyes solution (as a textile wastewater) under visible and sun light irradiation. The prepared catalyst with high photocatalytic activity was immobilized on inexpensive and available sup-

port substrates by dip-coating method. This techniques are simple, cheap and do not require complicated tools. The use of TiO_2 in stabilized mode (thin film) is extremely important for industrial application since it does not need extra separation steps during the photodecomposition reactions. EDX results confirmed the presence of Sr, S and N dopants in TiO_2 structure. This study shows that pH higher than 5.5 and photoreactor flow rate of 32 ml/min are the best parameters for high efficient azo dye photodegradation. Furthermore, immobilized catalyst was stable and repeatable, therefore can be used for long times.

ACKNOWLEDGEMENTS

The authors thank the University of Kashan, Iran for financial support of this work with Grant No. 2564513.

REFERENCES

1. S. Y. Lee and S. J. Park, *J. Ind. Eng. Chem*., **19**, 1761 (2013).
2. K. Guesh, A. Mayoral, C. Marquez_Alvarez, Y. Chebude and I. Díaz, *Micropor. Mesopor. Mater*., **225**, 88 (2016).
3. B. Y. Chen, M. M. Zhang, C. T. Chang, Y. Ding, K. L. Lin, C. S. Chiou, C. C. Hsueh and H. Xu, *Bioresour. Technol*., **101**, 4737 (2010).
4. I. Arslan-Alaton and J. L. Ferry, *Dyes Pigm*., **54**, 25 (2002).
5. K. Golka, S. Kopps and Z. W. Myslak, *Toxicol. Lett*., **151**, 203 (2004).
6. S. Malato, P. Fernández-Ibáñez, M. I. Maldonado, J. Blanco and W. Gernjak, *Catal. Today*, **147**, 1 (2009).
7. M. Brienza, M. Mahdi Ahmed, A. Escande, G. Plantard, L. Scrano, S. Chiron, S. A. Bufo and V. Goetz, *Chemosphere*, **148**, 473 (2016).
8. M. Cheng, G. Zeng, D. Huang, C. Lai, P. Xu, C. Zhang and Y. Liu, *Chem. Eng. J*., **284**, 582 (2016).
9. H. Suzuki, S. Araki and H. Yamamoto, *J. Water. Proc. Eng*., **7**, 54 (2015).
10. P. M. Rao, L. Cai, C. Liu, I. S. Cho, C. H. Lee, J. M. Weisse, P. Yang and X. Zheng, *Nano. Lett*., **14**, 1099 (2014).
11. A. Kubacka, M. Fernández-García and G. Colón, *Chem. Rev*., **112**, 1555 (2011).
12. M. A. Rauf and S. S. Ashraf, *Chem. Eng. J*., **151**, 10 (2009).
13. C. M. Malengreaux, G. M. L. Leonard, S. L. Pirard, I. Cimieri, S. D. Lambert, J. R. Bartlett and B. Heinrichs, *Chem. Eng. J*., **243**, 537 (2014).
14. A. Ajmal, I. Majeed, R. N. Malik, H. Idriss and M. A. Nadeem, *RSC Adv*., **4**, 37003 (2014).
15. U. I. Gaya and A. H. Abdullah, *J. Photochem. Photobiol. C Photochem. Rev*., **9**, 1 (2008).
16. D. S. Bhatkhande, V. G. Pangarkar and A. A. C. M. Beenackers, *J. Chem. Technol. Biotechnol*., **77**, 102 (2001).
17. N. M. Mahmoodi, M. Arami and N. Yousefi-Limaee, *J. Hazard. Mater. B*., **133**, 113 (2006).
18. I. Ivanova, J. Schneider, H. Gutzmann, J. O. Kliemann, F. Gärtner, T. Klassen, D. Bahnemann and C. B. Mendive, *Catal. Today*, **209**, 84 (2013).
19. H. Zangeneh, A. A. L. Zinatizadeh, M. Habibi, M. Akia and M. Hasnain Isa, *J. Ind. Eng. Chem*., **26**, 1 (2015).
20. S. S. Umare, A. Charanpahari and R. Sasikala, *Mater. Chem. Phys*., **140**, 529 (2013).
21. S. Palmas, A. Da Pozzo, M. Mascia, A. Vacca and P. C. Ricci, *Chem. Eng. J*., **211-212**, 285 (2012).
22. C. M. Malengreaux, G. M.-L. Léonard, S. L. Pirard, I. Cimieri, S. D. Lambert, J. R. Bartlett and B. Heinrichs, *Chem. Eng. J*., **243**, 537 (2014).
23. R. Asahi, T. Morikava, T. Ohwaki, K. Aoki and Y. Taga, *Science*, **293**, 269 (2001).
24. S. Naraginti, T. V. L. Thejaswini, D. Prabhakaran, A. Sivakumar, V. S. V. Satyanarayana and A. S. Arun Prasad, *Spectrochim. Acta A*., **149**, 571 (2015).
25. U. G. Akpan and B. H. Hameed, *Appl. Catal. A-Gen*., **375**, 1 (2010).
26. T. K. Tseng, Y. S. Lin, Y. J. Chen and H. Chu, *Int. J. Mol. Sci*., **11**, 2336 (2010).
27. M.-C. Yang, T.-S. Yang and M.-S. Wong, *Thin Solid Films*, **469-470**, 1 (2004).
28. R. S. Sonawane, B. B. Kale and M. K. Dongare, *Mater. Chem. Phys*., **85**, 52 (2004).
29. F. Zahedi, M. Behpour, S. M. Ghoreishi and H. Khalilian, *Sol. Energy*, **120**, 287 (2015).
30. M. Behpour and V. Atouf, *Appl. Surf. Sci*., **258**, 6595 (2012).
31. M. Pelaez, N. T. Nolan, S. C. Pillai, M. K. Seery, P. Falaras, A. G. Kontos, P. S. M. Donlop, J. W. J. Hamilton, J. A. Byrne, K. O'Shea, M. H. Entezari and D. D. Dionysiou, *Appl. Catal. B-Environ*., **125**, 331 (2012).
32. J. Zhang, P. Zhou, J. Liu and J. Yu, *Phys. Chem. Chem. Phys*., **16**, 20382 (2014).
33. L. Ma, W. Xu, S. Zhu, Z. Cui, X. Yang and A. Inoue, *Mater. Chem. Phys*., **170**, 186 (2016).
34. D. P. Macwan, P. N. Dave and S. Chaturvedi, *J. Mater. Sci*., **46**, 3669 (2011).
35. D. C. Hurum, A. G. Agrios, K. A. Gray, T. Rajh and M. C. Thurnauer, *J. Phys. Chem. B*., **107**, 4545 (2003).
36. R. Rattanakam and S. Supothina, *Res. Chem. Intermed*., **35**, 263 (2009).
37. H. Mamane, I. Horovitz, L. Lozzi, D. Di-Camillo and D. Avisar, *Chem. Eng. J*., **257**, 159 (2014).
38. S. Sood, A. Umar, S. K. Mehta, A. S. K. Sinha and S. K. Kansal, *Ceram. Int*., **41**, 3533 (2015).
39. F. Zahedi, M. Behpour, S. M. Ghoreishi and H. Khalilian, *Sol. Energy*, **120**, 287 (2015).
40. I. K. Konstantinou and T. A. Albanis, *Appl. Catal. B-Environ*., **49**, 1 (2004).
41. S. H. Hsieh W. J. Chen and C. T. Wu, *Appl. Surf. Sci*., **340**, 9 (2015).